Hindawi
Geofluids
Volume 2022, Article ID 2249766, 12 pages
https://doi.org/10.1155/2022/2249766

Research Article

Experimental and Numerical Simulation Study on Shear Strength and Secondary Particle Breakage of Coarse Sand with Different Dry Densities

Rui Luo,[1] **Fangcai Zhu**,[1] **Qing Liu**,[1] **Shaolong Zhang**,[2] **Binbin Wu**,[2] **Yaxin Shang**,[2] **and Qi Chen**[2]

[1]*School of Civil Engineering, Hunan University of Technology, Zhuzhou, Hunan 412007, China*
[2]*2nd Engineering Co. Ltd., China Railway Beijing Engineering Group Co. Ltd., Changsha, Hunan 410116, China*

Correspondence should be addressed to Fangcai Zhu; zhufangcai@163.com

Received 30 June 2022; Accepted 24 August 2022; Published 29 September 2022

Academic Editor: Dongdong Ma

In order to guarantee perpendicularity of rotary cast-in-place pile in Karst areas, filling, like sand, etc., is commonly used between the inner steel casing and the outer steel sleeve; while the outer steel sleeve is pulled out or a vertical load is applied on the top of the pile, the sand will move, contact, and push against each other, which leads to recrushing; therefore, shear characteristics and secondary breakage are a meaningful problem to study with regard to the influence of different sand densities. Through experimental direct shear tests, with different dry densities, shear stress versus shear displacement curves are obtained and internal friction angles are analyzed. The results show that internal friction angles increase along with increment of dry densities; more interesting is that the secondary breakage ratio also increases. A comparative numerical 2D model is set up using PFC2D, with lower porosity used to simulate a large dry density, and similar results are obtained, that is to say, with increase of dry densities, internal friction angles also increase.

1. Introduction

The pile foundation of a super large bridge in the Guinan high-speed railway adopts the construction technology of a full-sleeve full-rotary bored pile. There are two steel sleeves inside and outside in the construction process. The outer steel casing has to be pulled out. In order to ensure the verticality of the pile body, gravel is used to fill the gap between the pile body and the casing. During the process of casing extraction, gravel is used to fill the gap between the two. The displacement of the casing relative to the pile has a shear effect on the gravel. In the indoor pile foundation model experiment, the coarse sand of 1.18 mm-3.36 mm is selected to replace the gravel. Therefore, it is necessary to further explore the influence of the coarse sand with this particle size on the stability of pile foundation and conduct direct shear test [1, 2] on the coarse sand with this particle size. Through the shear test of coarse sand under different dry density conditions, the influence of the dry density of coarse sand on the internal friction angle and secondary crushing was studied, and the numerical simulation based on PFC software was carried out for comparison and verification.

According to Li et al. [3], through the establishment of the numerical simulation model of sandy soil, the approximate thickness of the shear zone is 10.37 times the average diameter of particles. Yang and Li [4] used PFC3D to simulate the shear experiments of sand soil with different shapes of particles and concluded that different shapes of particles had significant effects on the shear strength. Lei et al. [5] used discrete element software to systematically study the causes and laws of rock failure in the soil-rock mixture. Sun [6] studied the mechanical behavior of standard sand direct shear test from the aspects of particle shape, stiffness, porosity, and friction coefficient. Xu et al. [7] used super particles composed of multiple unit balls to simulate the direct shear test of sandy pebble soil and studied the shear performance of sandy pebble soil. Sadek et al. [8] simulated soil direct shear test by PFC3D and predicted soil shear behavior

according to shear stress and shear displacement. Zhang et al. [9] used the particle discrete element theory and PFC2D software to study the shear strength of the soil-rock mixture from the aspects of rock content and bond strength. Jia et al. [10] established a direct shear test model of the soil-to-rock mixture based on PFC3D software and concluded that the stone content of the soil-to-rock mixture and the lithology of the stone have an obvious influence on the shear strength. Xue et al. [11] used PFC2D to compare the results of the numerical simulation test and indoor test to analyze the mechanical properties and strain hardening effect of colluvial mixtures, and the two test conclusions are consistent.

By comparing previous research [12–14], it is found that there are few studies on the secondary crushing of sand in the shear test. This paper compares the indoor direct shear test with the PFC numerical simulation test. It is found that the dry density of the experimental sand affects the internal friction angle and the particle crushing value, and the growth trend of the crushing value shows a power function increase.

2. Laboratory Direct Shear Test

2.1. Test Materials and Equipment. Shear tests are widely used in the research fields of soil mechanics [15, 16] and rock mechanics [17–20]. According to the soil engineering classification specified in the standard for "Geotechnical Test Methods" [21] GB/T50123-2019 issued by the Ministry of Water Resources of the People's Republic of China, coarse sand is used as the research object in this test. The particle diameter range is 1.18 mm to 2.36 mm, as shown in Figure 1. Direct shear tests were carried out using the ZJ strain-controlled direct shear apparatus (see Figure 2). The instrument consists of a computer data acquisition and processing system and a quadruple shear main body. Shear tests under different vertical pressures are realized by lever action, and shear tests of four specimens can be performed simultaneously. In the working operation, the computer automatic acquisition numerical control system is mainly responsible for the input of control data before and during the shearing process, so as to achieve the effect of control variables. The instrument can control the selection of the shear rate, vertical load, direct shear, overlapping ring shear, etc. At the same time, it has the ability to collect and analyze the horizontal displacement, vertical displacement, shear stress, shear time, motor frequency, and other values in the shear process and draw images autonomously. The main part of the direct shear is mainly composed of horizontal loading system, vertical loading lever system, upper and lower shear box, data acquisition device, etc. The shear box is cylindrical with a diameter of 61.8 mm and a height of 20 mm and is divided into upper and lower layers. The specific technical parameters are as follows: the maximum vertical load is 400 kPa; the maximum horizontal shear force is 1.2 kN; the automatic control shear rate is 2.4, 0.8, 0.1, and 0.02 mm/min; and the leverage ratio is 1 : 12.

Figure 1: 1.18 mm~2.36 mm coarse sand.

Figure 2: Microcomputer-controlled direct shear apparatus.

2.2. Experimental Scheme. In order to study the shear characteristics of coarse sand under different dry densities, the dry density of coarse sand was measured by the fixed volume method and shaking table method. The results are shown in Table 1. Through direct shear tests on six kinds of coarse sand with different dry densities, each group applies vertical pressure by loading different numbers of weights. The vertical pressures of the same group of tests are 100 kPa, 200 kPa, 300 kPa, and 400 kPa. The shear rate is 0.8 mm/min. This experiment was carried out in strict accordance with the requirements of the direct shear test part of the "Test Methods of Soils for Highway Engineering" issued by the Ministry of Transport of the People's Republic of China [22].

(1) Select the coarse sand with the particle diameter between 1.18 mm and 2.36 mm and put it into the oven for drying for 6 hours

(2) The upper and lower shear box is installed, and the dried coarse sand (75 g) is poured into the shear box. A hardwood block is placed on the surface of the sample, and the hand is tapped gently to make the sample reach the required dry density, and then, the hardwood block is removed

(3) Apply 100 kPa, 200 kPa, 300 kPa, and 400 kPa loads at the vertical position to shear; after the direct shear test is completed, use a 1.18 mm sieve and weigh the weight with a particle size less than 1.18 mm

Firstly, the coarse sand with particle diameter between 1.18 mm and 2.36 mm was put into the oven for drying for 6 hours as required. Then, the upper and lower shear box is installed, and 75 g of dry test sand is weighed and poured into the shear box. A hardwood block is placed on the surface of the sample, and the hand is tapped gently to make the sample meet the required dry density, and then, the hardwood block is removed. Finally, the vertical loads of 100 kPa, 200 kPa, 300 kPa, and 400 kPa are installed on the

Table 1: Six groups of dry density values.

Group	1	2	3	4	5	6
Dry density	1.29 g/cm^3	1.35 g/cm^3	1.40 g/cm^3	1.45 g/cm^3	1.50 g/cm^3	1.55 g/cm^3

top of the shear. After the completion of the direct shear test, the experiment sand under these four vertical loads is screened with a 1.18 mm screen, and the weight with a particle size less than 1.18 mm is weighed.

3. Analysis of Direct Shear Test Results

The shear stress-shear displacement relationship curves at six different dry densities were obtained according to the indoor direct shear test, as shown in Figure 3 below.

According to the shear stress-shear displacement relationship curve in Figure 3, it can be found that the shear strength of the experiment sand increases with the increase of the vertical pressure. At the initial stage of specimen shear, the shear stress increases sharply with the increase of shear displacement, and this change gradually decreases with the test. When the shear stress reaches the peak value, the shear stress-shear displacement relationship curve becomes smooth and the slope approaches 0.

3.1. Effect of Different Dry Densities on Internal Friction Angle. Using the peak shear stress in Figure 3 and Mohr-Coulomb strength theory, the internal friction angle and cohesion under six groups of dry densities can be calculated, as shown in Table 2 below. The sand used in this test has been dried before the direct shear test, and there is no clay component. Therefore, there is no cohesion. The negative cohesion in the following table is caused by the error in curve fitting.

According to the data in Table 2 above, the internal friction angle-dry density curve can be drawn by taking the dry density as the ordinate and the internal friction angle as the abscissa, as shown in Figure 4 below.

After analyzing the growth trend in Figure 4, it can be concluded that the internal friction angle of coarse sand increases gradually with the increase of dry density. After fitting the scatter plot, it is concluded that the growth trend basically shows a linear growth. However, when approaching the maximum dry density, the increasing trend of the internal friction angle slows down slightly. With the increase in dry density, the gap between particles will become smaller and smaller, and the accumulation will be more compact. The contact area between particles will also increase, thus increasing the friction force and the internal friction angle. When the dry density is closer to the maximum dry density, the closeness between particles gradually approaches the limit state. The increase of internal friction angle also appears as a slow state.

3.2. Effect of Different Dry Densities on Crushing Value. The crushing value P is a ratio describing the degree of particle breakage. After each group of shear tests was completed, the sand used in the tests under different vertical pressures was screened, and the aperture of the screen was 1.18 mm. After the screening was completed, the mass m_i of residual sand in the screen was weighed. In this paper, the crushing value is defined as the ratio of the particle mass difference before and after the test to the particle mass before the test, namely,

$$P = \frac{m_0 - m_1}{m_0}. \tag{1}$$

Among them, m_0 represents the quality of the particles before the test and m_1 denotes the quality of particles after screening.

Based on the above formula, the crushing values of each vertical pressure under different dry densities are calculated, as shown in Table 3.

Taking the crushing value of particles as ordinate and dry density as abscissa, the relationship curve between dry density and crushing value is obtained by fitting the scatter diagram of crushing value of different dry densities, as shown in Figure 5 below.

It can be concluded from Figure 5 that the particle breakage is different under different dry densities. The greater the dry density, the greater the crushing degree of the sample. And the increasing amplitude of the crushing value under different dry densities is also increasing. With the increase of dry density, the gap between particles is smaller and smaller, and the compactness of the specimen is also larger and larger. The resistance received by the specimen in the shear process is also increased. Therefore, the degree of particle breakage under the action of external force increases, and the breakage value also increases.

3.3. Effect of Different Vertical Pressures on Breaking Value. According to the data in Table 3 and taking the vertical pressure as the abscissa and the crushing value of particles as the ordinate, the relationship curve between the crushing value and the vertical pressure is drawn, as shown in Figure 6 below.

It can be concluded from Figure 6 that the crushing degree of particles increases with the increase of vertical pressure. However, when the increase of vertical pressure is constant, the variation range of crushing values is larger. In each group of tests, the crushing value of 400 kPa vertical pressure has a greater range of change than the several previous pressures. The variation range is especially obvious when the sample is at the maximum dry density. Under the same dry density, the increase of vertical pressure will reduce the void ratio between particles, and the contact between particles is closer. Therefore, the friction area between particles in the shear process will increase, and the crushing value will also increase with increase of the crushing degree.

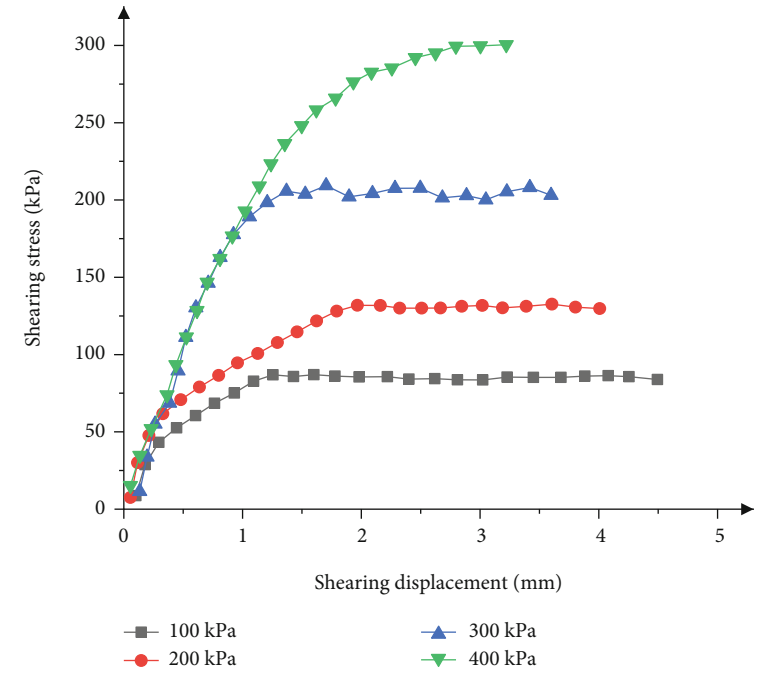

(a) Dry density 1.29 g/cm^3

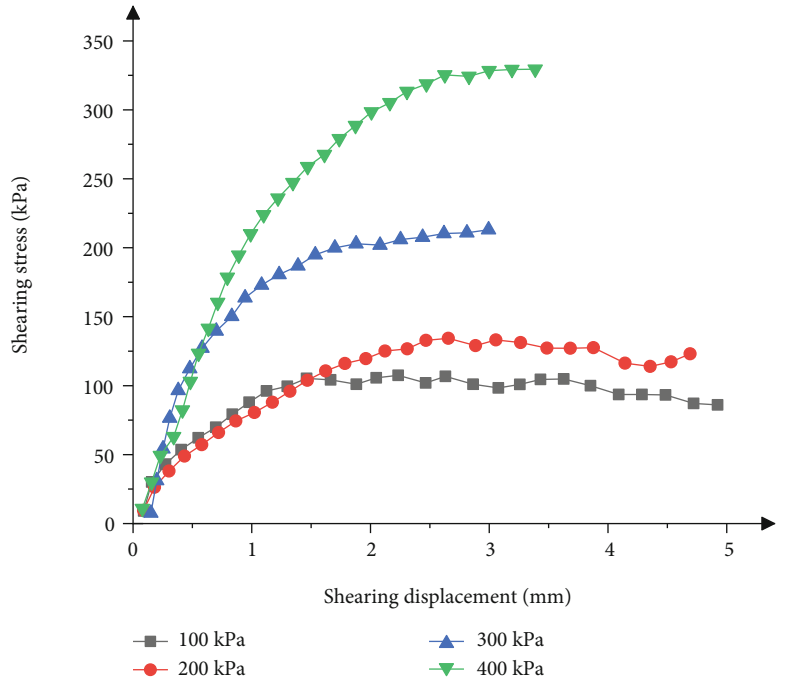

(b) Dry density 1.35 g/cm^3

Figure 3: Continued.

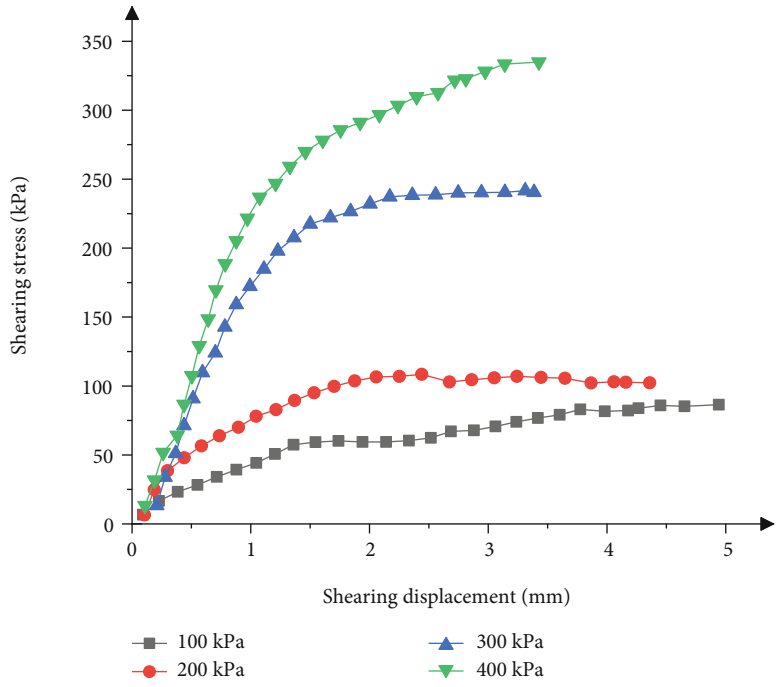

(c) Dry density 1.40 g/cm^3

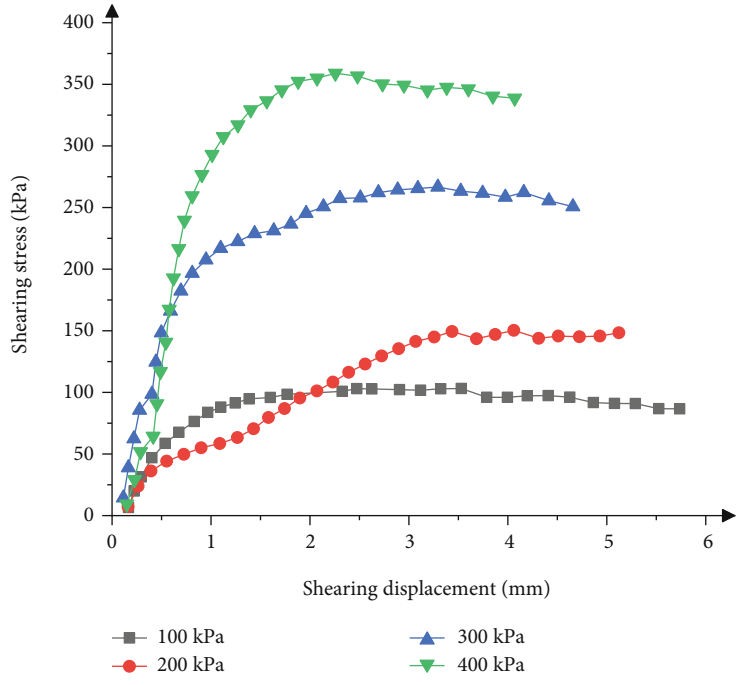

(d) Dry density 1.45 g/cm^3

Figure 3: Continued.

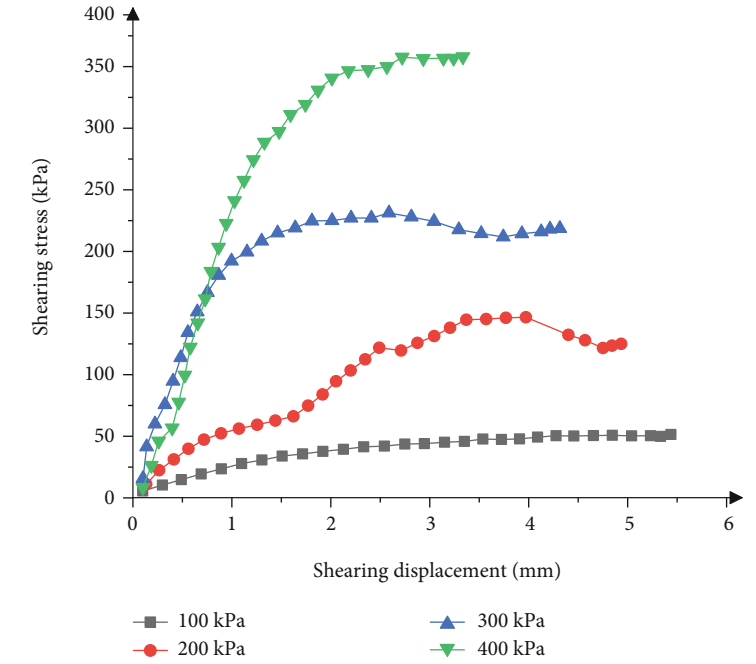

(e) Dry density 1.50 g/cm^3

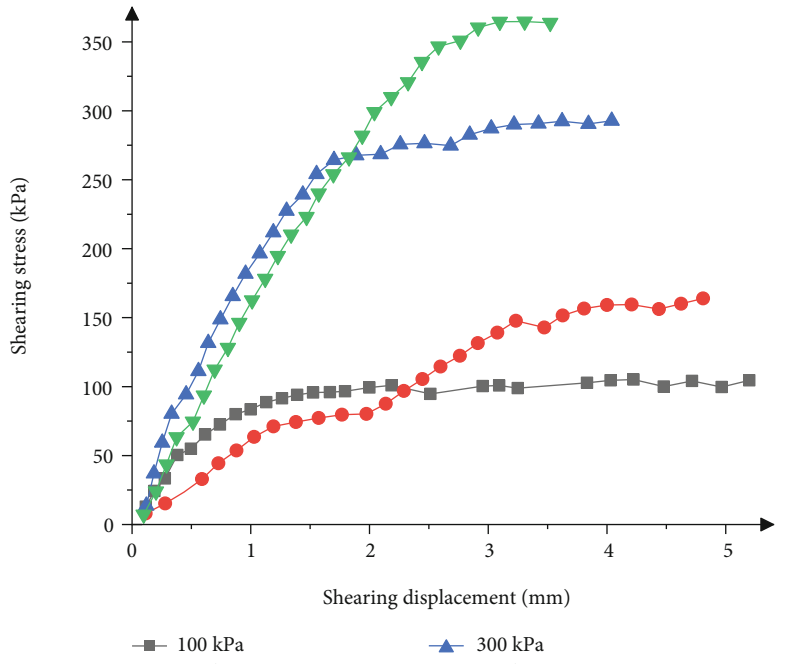

(f) Dry density 1.55 g/cm^3

Figure 3: The relationship curve between shear stress and shear displacement in direct shear test.

Table 2: Internal friction angle and cohesion at different dry densities.

Dry density (ρ_d/g/m^3)	1.29	1.35	1.40	1.45	1.50	1.55
Angle of internal friction (φ/°)	32.6	36.9	39.9	41.4	43.3	45.1
Force of cohesion (c/kPa)	25.8	10	-17.2	-9.2	-44.7	-46.6

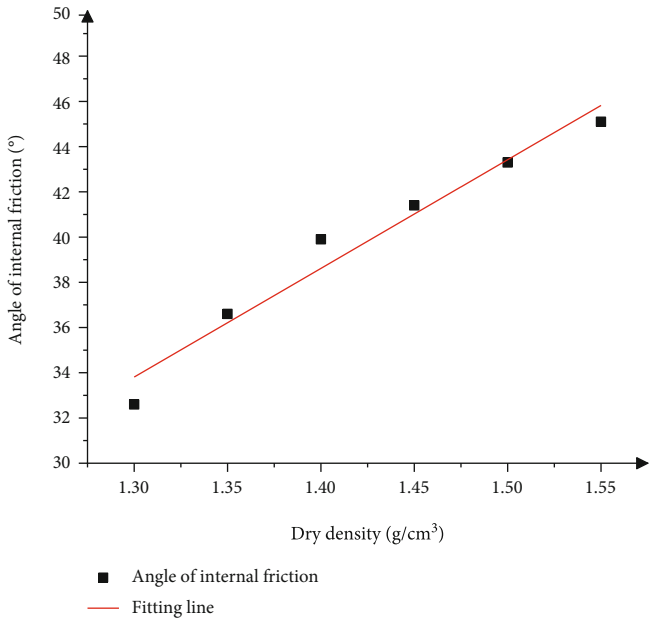

Figure 4: Curve of relationship between internal friction angle and dry density.

Table 3: Breakage values of particles in the direct shear test.

Dry density (ρ_d/g/m$^{3)}$	Crushing value (%)			
	100 kPa	200 kPa	300 kPa	400 kPa
1.29	3.8	4.9	5.7	6.7
1.35	4.8	5.6	6.1	8.7
1.40	5.1	6.27	7.5	10.7
1.45	5.3	6.7	8.3	12.1
1.50	6.6	7.3	9.5	15.3
1.55	8.8	9.9	11.9	18.3

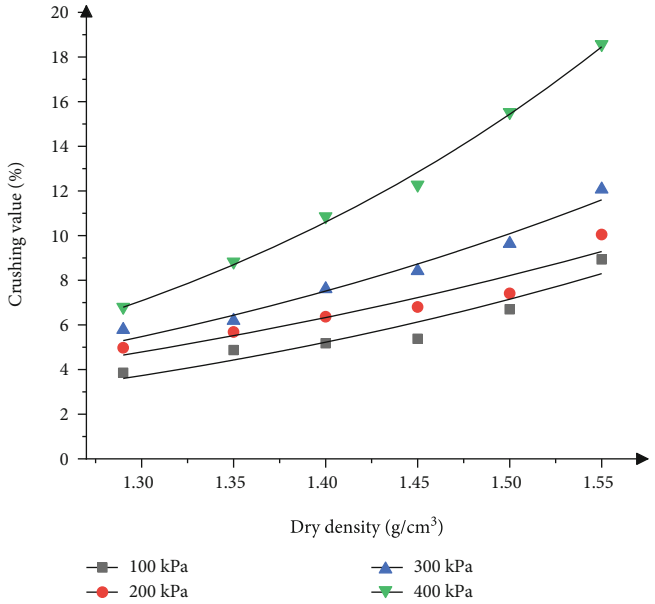

Figure 5: Curve of relationship between crushing value and dry density.

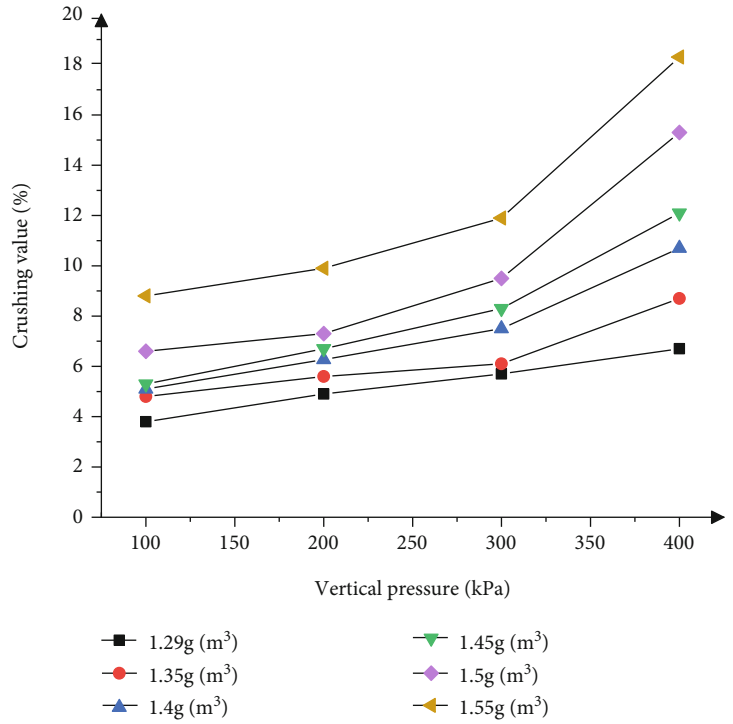

Figure 6: Curve of relationship between crushing value and vertical pressure.

4. PFC Numerical Simulation

4.1. PFC Numerical Simulation Model. This numerical simulation test uses PFC2D software developed by the Itasca Company for analysis [23, 24]. In order to make the numerical simulation test better match with the indoor shear test, the width and height of the shear box simulated in the PFC2D numerical simulation are 61.8 mm and 20 mm, respectively, and a total of 435 particles are generated. The simulated particle diameter is between 1.18 mm and 2.26 mm. In this simulation test, different dry densities are achieved by controlling the porosity between particles. When the range of particles is fixed, the smaller the porosity is, the larger the dry density is. The porosity set in this numerical simulation test is 0.18, 0.16, 0.14, 0.12, 0.10, and 0.08.

The WALL command was used to generate the shear box for the simulation test and then to generate the test particles inside the shear box. The maximum diameter of the particles was 2.26 mm, and the minimum diameter was 1.18 mm. The density of the particles was 2.58 g/cm^3. During the shear test, the friction between the particles was carried out, so the friction coefficient of the particles in the model test was 0.5 when they were in contact. After that, the pressure in the vertical direction is simulated by controlling the vertical movement of the upper and lower surfaces of the sample, and servo loading is carried out to keep the pressure in the vertical direction constant during the shear process. Finally, move the shear box and start the direct shear test. The numerical simulation model is shown in Figure 7. According to the theory of bulk elasticity, the particle contact stiffness is between 10^8 N/m and 10^9 N/m, and when the ratio of normal to tangential stiffness is 1 to 3, the model has good convergence [25]. After adjustment, the normal stiffness value is 2×10^8 N/m, the tangential stiffness value is 1×10^8 N/m, and the ratio between the two is 2. The microscopic parameters are shown in Table 4 below.

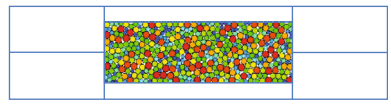

Figure 7: Numerical model of direct shear test through PFC2D.

Table 4: Microscopic parameters of PFC model.

Parameter	Value
Maximum radius (mm)	1.18
Minimum radius (mm)	0.59
Density (g/cm^3)	1.86
Porosity	0.3, 0.27, 0.25, 0.22, 0.2, 0.17
Normal stiffness (N/m)	2×10^8
Tangential stiffness (N/m)	1×10^8
Friction coefficient of particle	0.5
Friction coefficient of wall	0

4.2. Analysis of PFC Numerical Simulation Test Results. The test data were obtained by the PFC numerical simulation test, and the relationship curve between the shear stress and the shear displacement of the numerical simulation test was plotted, which was compared with the indoor direct shear test data. Through comparative analysis, the

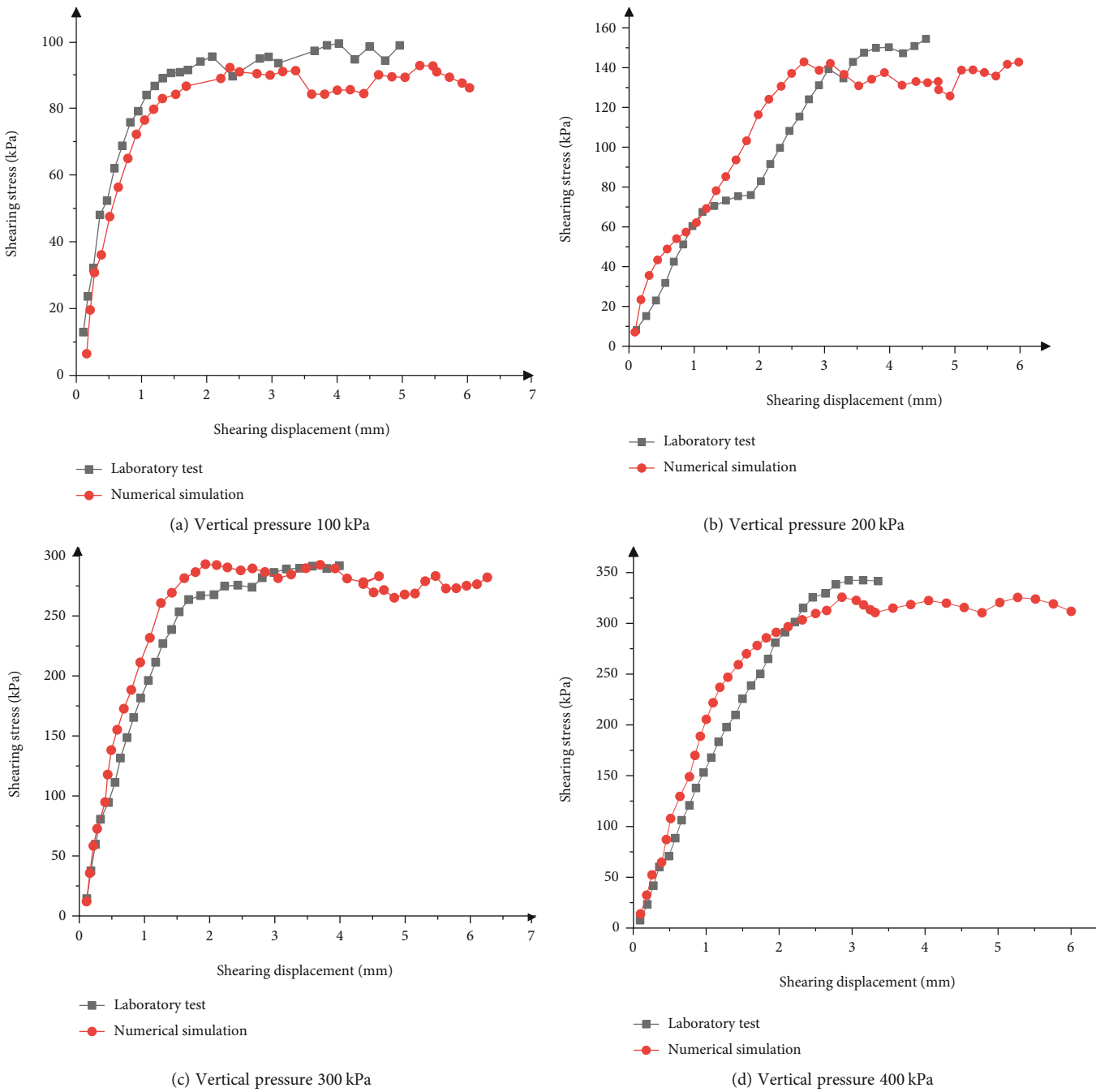

(a) Vertical pressure 100 kPa

(b) Vertical pressure 200 kPa

(c) Vertical pressure 300 kPa

(d) Vertical pressure 400 kPa

Figure 8: The shear stress-shear displacement curve of indoor test and numerical simulation.

Table 5: The results of direct shear test and numerical simulation are compared.

Property	Test results	PFC model experiment results
The peak value of shear stress (kPa)		
100 kPa	100.2	92
200 kPa	143.4	142
300 kPa	274.7	276
400 kPa	343.8	325
Angle of internal friction (°)	45.1	39.7

Table 6: The peak value of shear stress.

Vertical pressure (kPa)	The peak value of shear stress (kPa)					
	1.29 g/cm^3	1.35 g/cm^3	1.40 g/cm^3	1.45 g/cm^3	1.50 g/cm^3	1.55 g/cm^3
100	82	84	86	87	90	92
200	131	133	136	139	140	142
300	205	212	232	244	254	276
400	294	308	315	318	320	325

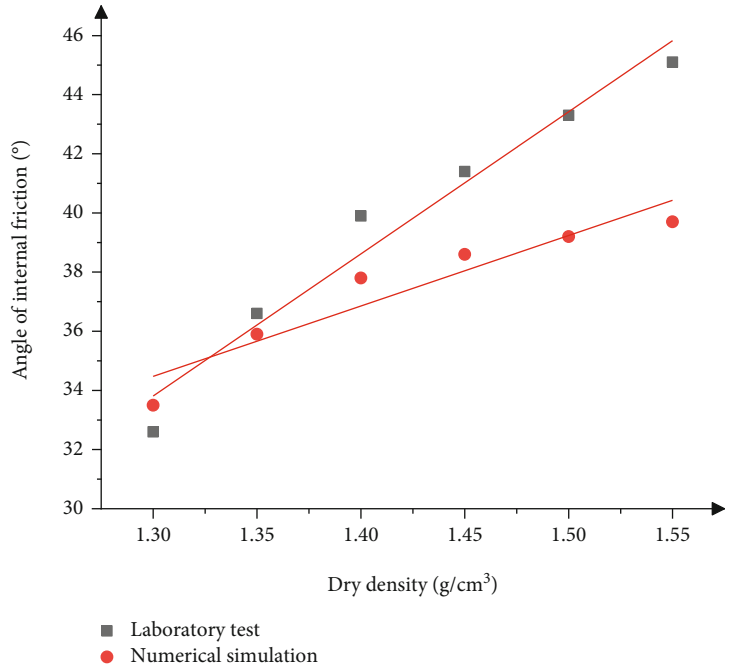

Figure 9: Internal friction angle-dry density curve of indoor test and numerical simulation test.

experimental results of the PFC numerical simulation are basically consistent with the results of the indoor direct shear test, and the trend of the curve is basically consistent, indicating that the effect of numerical simulation is ideal. The Figure 8 shows a comparison diagram of the shear stress-shear displacement curve between the numerical simulation test and the indoor direct shear test under different vertical pressures, with the dry density of 1.55 g/cm^3 as an example. The results of laboratory direct shear test and numerical simulation test are compared in Table 5 below.

The peak shear stress of each vertical pressure in the PFC numerical simulation test under different porosity is shown in Table 6. Then, according to the peak shear stress and Mohr-Coulomb strength theory, the internal friction angle under different porosities is calculated, and the comparison diagram of the internal friction angle-dry density curve between the indoor test and the PFC numerical simulation test is drawn, as shown in Figure 9.

By comparing the peak shear stress of the PFC numerical simulation test with that of the indoor direct shear test, it is found that the peak shear stress of the PFC numerical simulation test is generally lower than that of the indoor direct shear test. The reason for this phenomenon is that particles are broken in the process of the indoor direct shear test, and these broken particles enter the gap between large particles and large particles through the effect of vertical pressure, resulting in a decrease in the porosity of the sample and an increase in the contact area between particles. Therefore, the peak shear stress will be slightly higher than that of the PFC numerical simulation test. At the same time, the shear stress peak of the PFC numerical simulation test shows an upward trend under the same vertical pressure and different dry densities. In these six groups of dry density tests, the increase of dry density will affect the increase in internal friction. However, the slope of the fitting curve between the internal friction angle of the PFC numerical simulation test and the dry density was slightly lower than that of the indoor shear test, but the overall trend was consistent. In the previous groups of experiments, when the dry density of the same value is increased, the internal friction angle changes greatly. When the dry density approaches the maximum dry density, the increasing trend of internal friction angle slows down.

5. Conclusions

Based on experimental direct shear tests, shear characteristics is researched in detail and a comparative numerical

model is put forward using PFC2D; the following conclusions are drawn:

(1) Through direct shear tests, it is found that internal friction angles of coarse sand under different dry densities will increase with increment of dry densities; this trend will be slower while the dry density reaches a certain value

(2) With increment of dry densities, the secondary breakage ratio increases, on which normal stress has obvious influence; along with the increment of dry densities, this tendency becomes greater

(3) The results of the PFC2D numerical simulation test present a similar trend compared with experimental direct shear tests. The peak shear stress of the numerical simulation is slightly lower than that of the experimental results; also, a not-so-obvious trend is found through analysis of numerical results

Data Availability

All data and models generated or used during the study appear in the submitted article.

Conflicts of Interest

The authors declare that they have no conflicts of interest.

Acknowledgments

This research is sponsored by the Zhuzhou Joint Project of the Natural Science Foundation of Hunan Province (No. 2022JJ50087).

References

[1] Y. L. Zhao, C. S. Zhang, Y. X. Wang, and H. Lin, "Shear-related roughness classification and strength model of natural rock joint based on fuzzy comprehensive evaluation," *International Journal of Rock Mechanics and Mining Sciences*, vol. 137, article 104550, 2021.

[2] Q. Liu, Y. L. Zhao, L. M. Tang et al., "Mechanical characteristics of single cracked limestone in compression-shear fracture under hydro-mechanical coupling," *Theoretical and Applied Fracture Mechanics*, vol. 119, p. 103371, 2022.

[3] H. Li, Y. Lu, and K. Sun, "PFC numerical simulation of direct shear test on standard sand," *Journal of Shanghai University (natural science)*, vol. 23, no. 5, pp. 780–788, 2017.

[4] S. Yang and X. Q. Li, "Study on direct shear test simulation of PFC3d sand with different particle shapes," *Water Resources and Hydropower Technology*, vol. 50, no. 3, pp. 139–144, 2019.

[5] X. D. Lei, Z. P. Yang, H. Zhai, and Y. X. Hu, "Particle flow numerical research on factors influencing rock block breakage characteristics of soil-rock mixtures," *Journal of Engineering Geology*, vol. 28, no. 6, pp. 1193–1204, 2020.

[6] K. Sun, "Numerical simulation of direct shear test on standard sand," *Journal of Earthquake Engineering*, vol. 37, no. S2, pp. 185–190, 2015.

[7] G. Xu, Y. Yao, Y. J. Deng, D. G. Chen, and D. X. Wu, "Discrete element simulation of direct shear test of sandy pebble soil," *Sichuan Building Research*, vol. 42, no. 2, pp. 60–63, 2016.

[8] M. A. Sadek, Y. Chen, and J. D. Liu, "Simulating shear behavior of a sandy soil under different soil conditions," *Journal of Terramechanics*, vol. 48, no. 6, pp. 451–458, 2011.

[9] Z. P. Zhang, Q. Sheng, X. D. Fu, H. X. Luo, and L. Z. Dan, "Research on numerical direct shear test of soil-rock mixture based on particle flow code simulation," *Journal of Basic Science and Engineering*, vol. 29, no. 1, pp. 135–146, 2021.

[10] X. M. Jia, H. J. Chai, and Y. R. Zheng, "Mesomechanics research of large direct shear test on soil and rock aggregate mixture with particle flow code simulation," *Rock and Soil Mechanics*, vol. 31, no. 9, pp. 2695–2703, 2010.

[11] Y. D. Xue, Z. Q. Liu, and J. Wu, "Direct shear tests and PFC2D numerical simulation of colluvial mixture," *Geotechnical Mechanics*, vol. 35, no. S2, pp. 587–592, 2014.

[12] X. D. Lei, *Study on shear characteristics and fragmentation characteristics of soil-rock mixture, [Ph.D. thesis]*, Chongqing University, Chongqing, 2018.

[13] Y. L. Li and Y. H. Tian, "Experimental study on shear strength characteristics of silty sand under freezing and thawing conditions," *Transportation Soil Engineering in Cold Regions*, vol. 1, pp. 59–69, 2020.

[14] Y. Z. Wei, Z. H. Yao, X. L. Chong, J. H. Zhang, and J. Zhang, "Influence mechanism of structure on shear mechanical deformation characteristics of loess-steel interface," *Public Library of Science*, vol. 17, no. 2, pp. 1–33, 2022.

[15] Y. L. Zhao, L. Y. Zhang, W. J. Wang, J. Z. Tang, H. Lin, and W. Wan, "Transient pulse test and morphological analysis of single rock fractures," *International Journal of Rock Mechanics and Mining Sciences*, vol. 91, pp. 139–154, 2017.

[16] Y. Liu, S. R. Sun, J. H. Wei et al., "Mechanical characteristics of soil-rock mixtures containing macropore structure based on 3D modeling technology," *Journal of Mountain Science*, vol. 17, no. 9, pp. 2224–2240, 2020.

[17] Y. L. Zhao, Q. Liu, C. S. Zhang, J. Liao, H. Lin, and Y. X. Wang, "Coupled seepage-damage effect in fractured rock masses: model development and a case study," *International Journal of Rock Mechanics and Mining Sciences*, vol. 144, pp. 104822–104822, 2021.

[18] J. Wang, J. E. Dove, and M. S. Gutierrez, "Discrete-continuum analysis of shear banding in the direct shear test," *Geotechnique*, vol. 57, no. 6, pp. 513–526, 2007.

[19] W. J. Xu, X. Qiang, and R. L. Hu, "Study on the shear strength of soil–rock mixture by large scale direct shear test," *International Journal of Rock Mechanics and Mining Sciences*, vol. 48, no. 8, pp. 1235–1247, 2011.

[20] Y. F. Chen, H. Lin, Y. X. Wang, and Y. L. Zhao, "Damage statistical empirical model for fractured rock under freezing-thawing cycle and loading," *Geofluids*, vol. 2020, Article ID 8842471, 12 pages, 2020.

[21] Ministry of Water Resources of the People's Republic of China, *Standard for Soil Test Method (GB/T50123-2019)*, China Planning Press, Beijing, 2019.

[22] Ministry of Transport of the People's Republic of China, *Test Methods of Soils for Highway Engineering (JTG 3430—2020)*, China Communications Press, Beijing, 2020.

[23] X. Fan, X. D. Jiang, Y. X. Liu, H. Lin, K. H. Li, and Z. M. He, "Local stress distribution and evolution surrounding flaw and opening within rock block under uniaxial compression," *Theoretical and Applied Fracture Mechanics*, vol. 112, pp. 102914–102914, 2021.

[24] X. Fan, K. H. Li, H. P. Lai, Y. L. Xie, R. H. Cao, and J. Zheng, "Internal stress distribution and cracking around flaws and openings of rock block under uniaxial compression: a particle mechanics approach," *Computers and Geotechnics*, vol. 102, pp. 28–38, 2018.

[25] B. K. Mishra and S. P. Mehrotra, "Modelling of particle stratification in jigs by the discrete element method," *Minerals Engineering*, vol. 11, no. 6, pp. 511–522, 1998.